Thermally rounded depinning of an elastic interface on a washboard potential

A. B. Kolton and E. A. Jagla

Centro Atómico Bariloche, Instituto Balseiro, Comisión Nacional de Energía Atómica, CNEA, CONICET, UNCUYO,
Av. Bustillo 9500 R8402AGP S. C. de Bariloche, Río Negro, Argentina

The thermal rounding of the depinning transition of an elastic interface sliding on a washboard potential is studied through analytic arguments and very accurate numerical simulations. We confirm the standard view that well below the depinning threshold the average velocity can be calculated considering thermally activated nucleation of defects. However, we find that the straightforward extension of this analysis to near or above the depinning threshold does not fully describe the physics of the thermally assisted motion. In particular, we find that exactly at the depinning point the average velocity does not follow a pure power law of the temperature as naively expected by the analogy with standard phase transitions but presents subtle logarithmic corrections. We explain the physical mechanisms behind these corrections and argue that they are nonpeculiar collective effects which may also apply to the case of interfaces sliding on uncorrelated disordered landscapes.

I. INTRODUCTION

The depinning transition of elastic interfaces is a paradigmatic example of an out-of-equilibrium critical phenomenon. Its study is relevant for modeling diverse extended physical systems embedded in a quenched pinning potential. Often the pinning landscape acting in the interfaces is disordered such as in driven ferromagnetic [1] and ferroelectric [2,3] domain walls, tension-driven cracks [4–6], displacement of contact lines of liquid menisci [7–9], or earthquakes [10,11]. In other cases the pinning landscape can be highly correlated or even periodic, such as the potential energy of the superconducting phase difference in long current-driven Josephson junctions [12] or as in the case of field-driven domain walls in artificial pinning potentials [13–15].

The basic phenomenology of depinning consists of an elastic manifold with an overdamped motion that interacts with a quenched potential energy landscape that tends to trap the interface in configurations in which the potential energy is minimized. When a uniform external driving force is applied, the interface remains pinned in a local minimum of the tilted energy potential if the amplitude of the driving force is below some well-defined threshold, whereas otherwise it sets in a steady state of motion with a well-defined average velocity. The threshold value of the applied driving force defines the depinning force of the system f_c. When the driving force is slightly above the depinning threshold the velocity of the interface is expected to grow as a power law of the excess driving above the threshold value. This is just one indication that the kind of phenomenon occurring near f_c can be characterized as a (nonequilibrium) phase transition with critical properties [16–18].

The existence of a sharp depinning transition as a function of the driving force of an elastic interface depends crucially on the fact that thermal effects are negligible. If thermal fluctua-

tions are important, then the depinning transition is smeared out, as for any finite applied force the interface can eventually jump forward via thermally activated events over energy barriers, and hence the average velocity becomes different from zero for any nonzero driving force. It has been proposed that the effect of a small temperature on the depinning transition can be accounted for through an appropriate generalization of the scaling theory used at $T = 0$. In this respect, it has been suggested, either following a naive analogy with standard equilibrium phase transitions or by phenomenological nucleation theory arguments, that the effect of temperature on the depinning transition can be characterized by the value of a "thermal rounding" exponent ψ that describes the average velocity v right at f_c as a function of temperature, namely $v(f_c, T) \sim T^\psi$. Regarding the velocity as the order parameter, the force as the control parameter and the temperature as a "symmetry-breaking field destroying the pinned phase" [19] such scaling proposal for the rounded depinning transition is analogous to the scaling with field H of the equilibrium Ising model magnetization M at the critical temperature T_c, $M(T_c) \sim H^{1/\delta}$ with $\delta > 0$, to cite the simplest example. However, the precise determination of the value of ψ has proven to be quite tricky [20,21], its universality questioned [22], and there is not yet a rigorous proof that the naive thermal rounding scaling theory is even consistent, in contrast with the zero temperature dynamics [18,23–25] and the subthreshold creep dynamics [26–29].

In order to advance in the study of the thermal rounding of depinning-like transitions, we concentrate here in a case in which the zero-temperature limit provides an almost trivial result for the flux curve and where the effect of temperature can be treated in a very accurate if not rigorous manner. This is the case of an elastic manifold evolving on a periodic pinning potential, the same for all individual sites of the elastic manifold, also known as a "washboard potential." The model

is, on the other hand, the celebrated overdamped Sine-Gordon dynamical model which has been used to model many different physical phenomena, such as the motion of dislocations in the Peierls potential of a crystal [30] overdamped coupled pendula [31], the equilibrium roughening transition [32], crystal growth [33,34], vortex matter in layered superconductors [35–38], forced soliton gases [39], and overdamped long Josephson junctions driven by an external current [12]. The Sine-Gordon model is closely related to the Frenkel-Kontorova [40] and Prandtl-Tomlinson models relevant for nanotribology [41], and it may be also used to model the dynamics of the internal degrees of freedom of an extended magnetic domain wall describing the axial rotation of the local magnetization vector, relevant for spintronics [42–44]. A proper understanding of the depinning transition of the Sine-Gordon model per se is hence also very important, as it is, for instance, related to the onset of rotation of torque-driven coupled pendula, the onset of dissipation in superconducting systems such as Josephson junctions or vortex systems, or to the Walker breakdown in magnetic domain wall systems.

In this paper we show, both through analytic arguments and very accurate numerical simulations, that the effect of temperature at the depinning transition in this simple extended model cannot be accounted for by a simple one-parameter scaling and that it involves the appearance of subtle logarithmic corrections not precluded by any of the standard arguments made so far for the thermal rounding of the depinning transition. We thus expect that this qualitative behavior is not peculiar of the model but applies, for instance, to the more standard and complicated case of uncorrelated disorder.

II. MODEL

Consider an elastic interface (with short-range interactions) in d spatial dimensions, characterized by its position $h(r)$. The interface feels the effect of an underlying periodic potential $V(h)$ and an external force f. The dynamical equations of the system are [31]

$$\frac{\partial h(r,t)}{\partial t} = -\frac{dV(h)}{dh} + \nabla^2 h + f + \sqrt{T}\eta(t,r), \quad (1)$$

where temperature has been introduced through the use of a standard Langevin formalism, with the white noise η characterized by

$$\langle \eta(t,r)\rangle = 0, \quad \langle \eta(t,r)\eta(t',r')\rangle = 2\delta(t-t')\delta^d(r-r'). \quad (2)$$

At $T = 0$ the dynamics of the system greatly simplifies, as the interface becomes flat [45], and its global position h follows the one-particle equation,

$$\frac{\partial h}{\partial t} = -\cos(h) + f \quad (3)$$

[from now on we specialize to a potential of the form $V(h) = \sin(h)$]. For $f < f_c = 1$ the interface does not move, whereas for $f > f_c$ there is a finite average velocity. For f slightly above f_c, the velocity $v \equiv \langle \partial_t h \rangle$ scales as

$$v \sim \sqrt{f - f_c}, \quad (4)$$

which defines the flow exponent β [from $v \sim (f - f_c)^\beta$] as $\beta = 1/2$. At finite temperature this sharp continuous transi-

tion is smoothed and, at variance with the peculiar $T = 0$ case, the problem becomes a nontrivial collective problem. In the following sections we discuss the thermally activated dynamics below the depinning threshold for $|f - f_c| \ll f_c$ and then the subtle $f = f_c$ case at finite temperature.

III. ACTIVATED DYNAMICS SCALING NEAR THE DEPINNING THRESHOLD

The finite-temperature activation dynamics described by Eq. (1) well below f_c was studied in Ref. [31] and also in Ref. [46] using renormalization group methods. Here we will follow an approach that uses dimensional analysis mainly. Our aim is to calculate the value of v for finite temperature and for f very close to $f_c = 1$. If f is only slightly below 1, and T is very small [$T \ll (f_c - f)$], then the dynamics is dominated by thermal activation events in which patches of the interface (of linear size l_0 to be determined below) advance a definite spatial amount. These patches then grow in size deterministically.

We consider a d-dimensional system with periodic boundary conditions at very low temperature and assume that we start with a nearly flat interface resting in a local minimum of the tilted potential [$\sin(h) - fh$], with $f = f_c - \varepsilon$, and $\varepsilon \ll 1$. Then we can approximate the potential by $\varepsilon h - h^3/6$ near the transition point [47]. The local energy minimum is thus located at $h = -\sqrt{2\varepsilon}$, the maximum at $h = +\sqrt{2\varepsilon}$. Using this expansion in Eq. (1) the resulting dynamical equations that will describe the escape from the energy minimum can be written in a normalized form as

$$\frac{\partial h(r,t)}{\partial t} = \frac{h^2}{2} - \varepsilon + \nabla^2 h + \sqrt{T}\eta(t,r). \quad (5)$$

We first calculate the rate of nucleation of defects R (that make the interface advance) per unit of time and unit of volume of the system in a system with spatial extension L. R will depend on the two parameters T and ε present in Eq. (5) and also on L, i.e., we can write $R(T, \varepsilon, L)$. First we sketch a scaling analysis that allows to reduce the three-parameter dependence of R to a two-parameter dependence. Suppose we know the value of R for given values of T, ε and L. Then we scale all variables and parameters in Eq. (5) according to the following table:

$$\varepsilon \to \tilde{\varepsilon} \equiv k\varepsilon, \quad (6)$$

$$h \to \tilde{h} \equiv k^{1/2}h, \quad (7)$$

$$t \to \tilde{t} \equiv k^{-1/2}t, \quad (8)$$

$$r \to \tilde{r} \equiv k^{-1/4}r, \quad (9)$$

$$L \to \tilde{L} \equiv k^{-1/4}r, \quad (10)$$

$$T \to \tilde{T} \equiv k^{(6-d)/4}T, \quad (11)$$

where k is an arbitrary scaling factor. It is readily verified that tilde variables satisfy an equation formally identical to the original one. The above scaling means that the number of activation events in corresponding time and space intervals are equal for the original and the scaled equation. In concrete,

$$R(T, \varepsilon, L)[t][r]^d = R(\tilde{T}, \tilde{\varepsilon}, \tilde{L})[\tilde{t}][\tilde{r}]^d \quad (12)$$

or

$$R(T, \varepsilon, L) = R(k^{(6-d)/4}T, k\varepsilon, k^{-1/4}L)k^{-(d+2)/4}. \quad (13)$$

Since k is arbitrary we can choose $k \sim 1/\varepsilon$ to obtain

$$R(T, \varepsilon, L) = \varepsilon^{(d+2)/4}R\left[\frac{T}{\varepsilon^{(6-d)/4}}, 1, L\varepsilon^{1/4}\right]. \quad (14)$$

Alternatively, and assuming for simplicity the large system-size limit ($L\varepsilon^{1/4} \gg 1$), we can accommodate the previous expression as

$$R(T, \varepsilon) = T^{\frac{d+2}{6-d}}\mathcal{F}\left[\frac{\varepsilon^{(6-d)/4}}{T}\right], \quad (15)$$

where we have dropped the L dependence and defined the unknown function $\mathcal{F}$ as

$$\mathcal{F}(x) \equiv x^{\frac{d+2}{6-d}}R(1/x, 1, \infty). \quad (16)$$

Equation (15) explicitly gives the two parameter form of $R(T, \varepsilon)$ in terms of an unknown function $\mathcal{F}$ of a single variable. While Eq. (14) shows the finite-size scaling effects, the existence of $\mathcal{F}$ guarantees a well-defined thermodynamic limit for the nucleation rate, when $L\varepsilon^{1/4} \gg 1$ or $LT^{1/(6-d)} \gg 1$.

The combination $\varepsilon^{(6-d)/4}/T$ in the argument of $\mathcal{F}$ suggests that $\varepsilon^{(6-d)/4}$ is actually a relevant energy scale of the problem and thus we will denote $\alpha = (6-d)/4$ as the "energy exponent." In fact, its physical meaning can be unveiled by a simple variant of the "droplet" argument [35,48]. Suppose we want to estimate what is the optimal linear size l_0 of a patch of the surface to jump the energy barrier implied by the force density term $h^2/2 - \varepsilon$ in Eq. (5). Assuming simple excitations, solely characterized by its linear size l_0 and displacement h, the additional elastic energy of order $(h/l_0)^2 l_0^d$ must be added to the potential energy $(\varepsilon h - h^3/6)l_0^d$, yielding the patch energy near f_c,

$$E(h, l_0) \sim (\varepsilon h - h^3/6)l_0^d + (h/l_0)^2 l_0^d/2. \quad (17)$$

For any $0 < d < 6$ the excitation energy $E(h, l_0)$ has an extremum at $l_0^* \sim \varepsilon^{-1/4}$ and $h^* \approx \sqrt{\varepsilon}$, yielding the exact scaling result

$$E^* \equiv E(h^*, l_0^*) \sim \varepsilon^{(6-d)/4}. \quad (18)$$

This confirms the physical connection with Eq. (15). For $d < 2$ such an extremum is a saddle point and E^* is the minimal barrier to advance forward. The optimal size $l_0^* \sim \varepsilon^{-1/4}$ is such that the small ($l_0 \ll l_0^*$) frequently activated patches are futile (i.e., they are quickly reversed) while large-enough ($l_0 > l_0^*$) patches trigger irreversible forward jumps of the whole segment. This physical argument also makes clear that the function $\mathcal{F}$ in Eq. (15) will contain a dominant factor $\exp[-C\varepsilon^{(6-d)/4}/T]$ corresponding to an Arrhenius factor for the activation of these kind of optimal patches, provided $T \ll \varepsilon^{(6-d)/4}$ and under the assumption that the considered segment size is larger than l_0 [49].

All the previous scaling analysis can be presented also for a nonquadratic force minimum, replacing $h^2 \to h^\gamma$ in the right-hand side of Eq. (5), yielding (in the limit of large sizes $LT^{\frac{\gamma-1}{2\gamma-\gamma d+2}} \gg 1$, see Appendix A),

$$R(T, \varepsilon) = T^\sigma \mathcal{F}(\varepsilon^\alpha/T), \quad (19)$$

with

$$\sigma = \frac{(\gamma - 1)(d + 2)}{2(\gamma + 1) - (\gamma - 1)d}, \quad (20)$$

$$\alpha = 2 - \frac{(2 + d)(\gamma - 1)}{2\gamma}. \quad (21)$$

Equation (19) reduces to Eq. (15) for $\gamma = 2$. In particular, Eq. (21) generalizes the energy exponent α. The above results are valid for estimating the thermally activated decay rate of an initially flat segment of the interface by the production of a single defect. We now analyze in more detail the simplest cases, namely the particle and the elastic string, keeping the standard $\gamma = 2$ for simplicity.

A. Single particle

For a single particle ($d = 0$) each activation event represents the jump over one barrier and leads to the advance of the particle by a finite amount 2π. This means that the velocity in the single-particle case will follow the scaling:

$$v_{d=0}(\varepsilon > 0, T) \sim R_{d=0} \sim T^{1/3}\mathcal{F}(\varepsilon^{3/2}/T). \quad (22)$$

The explicit form of the function $\mathcal{F}$ in Eq. (22) and then the form of v is in fact well known in the limit $\varepsilon > 0$, $T \ll \varepsilon^{3/2}$, which is the thermally activated regime. This corresponds to the Kramers problem of escape over a barrier. The velocity is simply proportional to the inverse of the escape time of a thermal particle in the potential well $\varepsilon h - h^3/6$. Kramers's formula applied to this case provides

$$v_{d=0}(T \ll \varepsilon^{3/2}) = 2\pi\sqrt{\varepsilon}\exp\left(-\frac{4\sqrt{2}}{3}\frac{\varepsilon^{3/2}}{T}\right). \quad (23)$$

This expression satisfies the scaling expression Eq. (22).

In the present single-particle case the scaling argumentation can be extended to negative (but small) ε, meaning f slightly above the critical value $f_c = 1$, since in this case the dynamics is also dominated by the bottlenecks near the points where v is very small. This means that Eq. (22) can also be used for $\varepsilon < 0$. In this case, there is a finite limit for the velocity as $T \to 0$, and for this to be the case $f(-x) \sim (-x)^{1/3}$ for $x \to \infty$, leading to

$$v_{d=0}(\varepsilon < 0, T = 0) \sim |\varepsilon|^{1/2}, \quad (24)$$

which is the expected result. Equation (22) used at $\varepsilon = 0$ also indicates that for a single particle $v_{d=0}(\varepsilon = 0, T) \sim T^\psi$, with a well-defined thermal rounding exponent $\psi = 1/3$ [21,50,51].

B. Elastic string

We now analyze the case $d = 1$, corresponding to an elastic string. Equation (15) becomes in this case

$$R_{d=1}(T, \varepsilon) = T^{3/5}\mathcal{F}(\varepsilon^{5/4}/T). \quad (25)$$

In $d = 1$ the relation between R and the velocity of the interface can be worked out as follows: R represents the rate of creation of kink-antikink pairs. Each kink or antikink moves at a velocity $\pm c$ [52] and then each of them contributes equally to the velocity, so the velocity is proportional to the number N of kink-antikink pairs present in the system. The equilibrium

value of N is obtained by balancing the creation of kinks ($\sim R$) to its annihilation rate, which (like a chemical reaction between two species) is proportional to N^2 [53]. Namely

$$\frac{dN}{dt} \sim R - N^2. \tag{26}$$

By requiring equilibrium ($dN/dt = 0$) we obtain

$$v \sim N \sim R^{1/2}. \tag{27}$$

Therefore,

$$v_{d=1}(T, \varepsilon) = T^{3/10} \mathcal{G}(\varepsilon^{5/4}/T), \tag{28}$$

where $\mathcal{G} \equiv \sqrt{\mathcal{F}}$. Alternatively, we can also write

$$v_{d=1}(T, \varepsilon) = \varepsilon^{3/8} \widetilde{\mathcal{G}}(\varepsilon^{5/4}/T). \tag{29}$$

This expression is consistent with the form found in Ref. [31], which can be written (in our notation and units and up to preexponential numerical constants) as

$$v_{d=1}(T, \varepsilon) \sim \frac{\varepsilon^{11/16}}{T^{1/4}} \exp\left[-\frac{24}{5}\frac{(2\varepsilon)^{5/4}}{T}\right]. \tag{30}$$

In Fig. 1 we test the scaling in Eq. (29) numerically by integrating Eq. (1) for $d = 1$ using finite differencing and the stochastic Euler method on L elastically coupled particles. As shown in Fig. 1(b) there is excellent agreement below the depinning threshold, i.e., for $\varepsilon > 0$. One remarkable thing about the scaling of Eq. (28) is that it is *not* compatible with the well-known behavior of v for negative ε (i.e., $f > 1$) and $T = 0$. In fact, if a T-independent limit is going to be extracted from Eq. (28), then this should be $v \sim |\varepsilon|^{3/8}$, which does not coincide with the known exact result $v(T = 0, \varepsilon < 0) \sim |\varepsilon|^{1/2}$. This incompatibility can be appreciated in the $\varepsilon < 0$ (i.e., $f > f_c$) part of Fig. 1(b), where clearly the curves do not collapse. The good collapse for $f > f_c$ is obtained rescaling ε with the same energy exponent, namely $\varepsilon/T^{1/\alpha} = (f - f_c)/T^{1/\alpha}$ with $\alpha = (6 - d)/4 = 5/4$ [31], but using $v/T^{2/5}$ in the vertical axis, in order to obtain $\beta = 1/2$ [Fig. 1(c)]. The conclusion is that a unique thermal rounding scaling is not valid in this problem for d equal to (or larger than) one. In particular, if we try to define a single thermal rounding exponent, then we should choose $\psi = 3/10$ from the $f < f_c$ part of the scaling, but $\psi = 2/5$ from the $f > f_c$ part. We will see below how this incompatibility manifests in the true form of $v(T)$ at $f = f_c$ having a nontrivial logarithmic correction.

IV. THERMAL ROUNDING OF THE DEPINNING TRANSITION

The results in Sec. III clearly show that a unique global scaling of the form

$$v = T^\psi \mathcal{F}(\varepsilon^\alpha/T) \tag{31}$$

is valid only for the simplest case of a single particle but does not apply to interfaces in finite dimensions.

For an extended interface the form of the activated dynamics scaling below f_c ($\varepsilon > 0$) cannot be extrapolated to the $\varepsilon < 0$ region. Moreover, the form of the velocity as a function of temperature predicted by Eq. (31) when $\varepsilon = 0$, namely
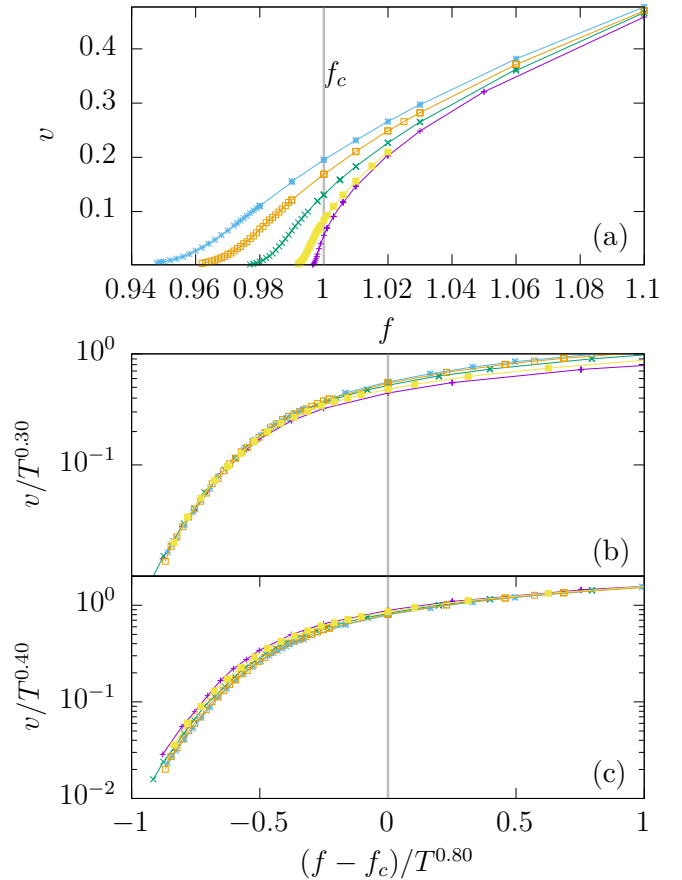
$$v \sim T^\psi \tag{32}$$

FIG. 1. Velocity force characteristics around the depinning threshold of an elastic string in the washboard potential at different temperatures $T = 0.003, 0.02, 0.03, 0.01, 0.001$. (a) Whole range around $f_c = 1$. Best scaling collapses just below the threshold $f \lesssim f_c$ (b) and just above the threshold $f \gtrsim f_c$ (c). The exponents are clearly different above and below threshold, in contrast with the one-particle case.

is not accurately satisfied, as we will show below. It turns out that this scaling has important logarithmic corrections that we will now address.

We will make a detailed analysis of the dynamics of the system right at the critical force f_c (i.e., $\varepsilon = 0$). Thus the model to be studied is that of Eq. (1) for a sinusoidal pinning potential at the critical force, namely

$$\frac{\partial h(r, t)}{\partial t} = -\cos(h) + 1 + \nabla^2 h + \sqrt{T}\eta(t, r), \tag{33}$$

as a function of temperature, in the $T \ll 1$ limit, where critical scaling functions and exponents are expected.

A. Single particle

To serve as a reference we start with the analysis of the single-particle case, that is, solving

$$\frac{dh}{dt} = -\cos(h) + 1 + \sqrt{T}\eta(t), \tag{34}$$

with $\langle \eta(t)\eta(t')\rangle = 2\delta(t - t')$. Figure 2 displays the numerically obtained evolution of $h(t)$ for different temperatures. We
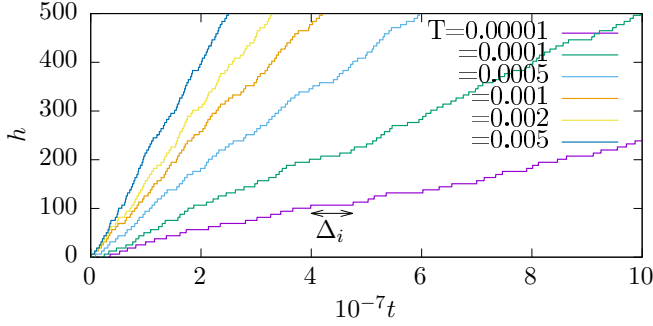
FIG. 2. Position-time plot for a single particle at the critical force, at different temperatures, as indicated. The motion proceeds by a sequence of jumps of size 2π separated by stochastic waiting times Δ_i.

clearly see that the dynamics proceeds through abrupt jumps between successive "bottlenecks" positions that occur when h is a multiple of 2π, at which the particle spends most of the time. These are the points at which the deterministic force on the particle vanishes. The average velocity as a function of temperature follows the prediction of Eq. (22) at $\varepsilon = 0$, namely $v \sim T^{1/3}$. However, we emphasize that this scaling applies not only to the average velocity (which is related to the average waiting time at the bottlenecks) but also to the whole distribution of time intervals spent at the bottleneck positions. This is shown in Fig. 3(a) where the cumulative probability distribution $F(\Delta, T)$ of the time intervals Δ spent at each bottleneck is calculated for different small temperatures [54]. As shown in Fig. 3(b) the results adjust perfectly to the scaling law

$$F(\Delta, T) = f(\Delta/T^{1/3}). \tag{35}$$

Therefore, for the average particle velocity $v \sim \overline{\Delta^{-1}}$ we get $v \sim T^{1/3}$, as it has been observed with high accuracy (see, for instance, Fig. 20 in Ref. [21]). This simply confirms that the particle accurately obeys the thermal rounding scaling of Eq. (32).

As shown in Figs. 3(c) and 3(d), $f(\Delta)$ displays an exponential decay at large Δ and a sort of "pseudogap" at small Δ, where $f(T^{1/3}\Delta)$ is almost zero. The existence of this "minimum time" for a jump [55] will play an important role in the analysis of the movement of the one-dimensional string that we consider in the following.

B. Elastic string

1. Kink-antikink dynamics at $f = f_c$

To gain insight in the form in which a one-dimensional elastic string moves at $f = f_c$, we solve numerically Eq. (33) for $d = 1$. In Fig. 4 we display a few snapshots of the configuration of the system in a well-equilibrated state, at slightly increasing times. We see a characteristic structure in which pieces of the interface are located at positions corresponding to the bottlenecks of the potential. For convenience we will number successive bottlenecks with an integer index ν, such that the interface stays at $h = 2\pi\nu$. Different pieces of the interface are connected through "kinks" in which the interface
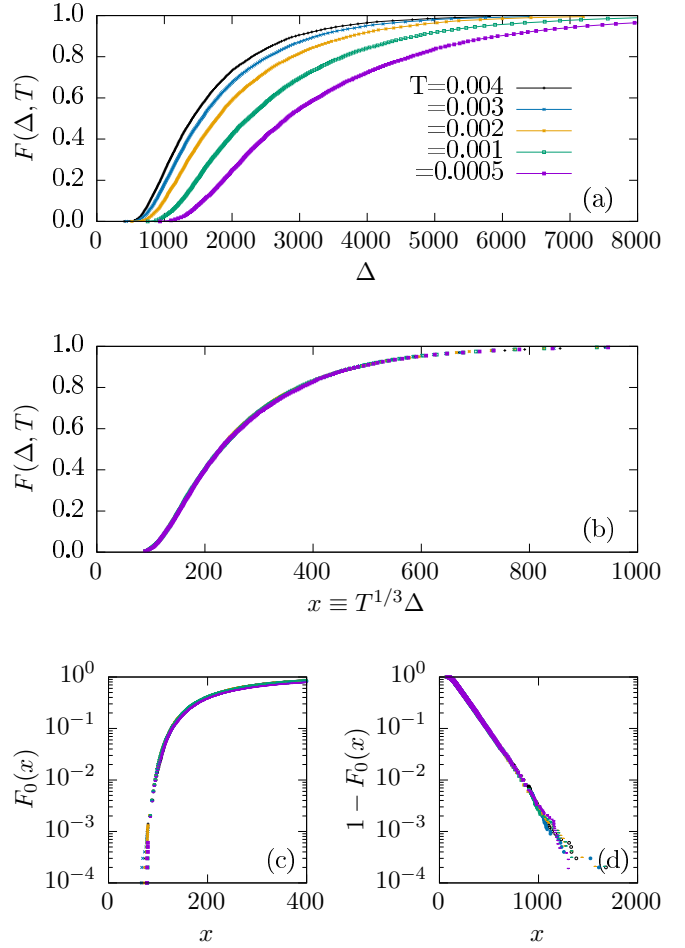

FIG. 3. (a) Cumulative distribution $[F(\Delta, T) \equiv \text{Prob}(\Delta_i < \Delta)]$ of the stochastic waiting times Δ_i (see Fig. 2) between successive jumps of a single particle ($d = 0$) in a tilted washboard potential, exactly at $f = f_c = 1$, for different temperatures. (b) The distribution can be collapsed onto a single curve by plotting it as a function of $T^{1/3}\Delta$. The left (c) and right (d) tails of the cumulative distribution highlight, respectively, the slower-than-exponential growth of the probability for short waiting times and its exponential decay for large waiting times.

passes from ν to $\nu \pm 1$, as again shown in Fig. 5(a). It is important to realize that the kinks move in a very deterministic and predictable way. In fact, as a piece of interface at position ν has a potential energy per site of $-2\pi\nu$, a kink connecting ν and $\nu + 1$ decreases its energy by moving in the direction that increases the extent at $\nu + 1$ an decreases that at ν. This produces that all kinks in the system move at a constant velocity $c \approx f_c \xi / 2\pi$ [31], where ξ is the kink width. For our numerical setup [Eq. (33)] we find $c \approx 0.24$, in consistence with $f_c = 1$ and the observed $\xi \approx O(1)$ (see Fig. 4), always in the direction of producing a net advance of the interface.

Figure 5(b) is an alternative and comprehensive view of kink movement in the system. It is a space-time plot of all kinks or antikinks trajectories in the system. As kinks move always at the velocity $\pm c$, their trajectories are seen as straight lines in Fig. 5(b). When kink and antikinks collide, they annihilate at the "Λ"-shaped points. In addition, kink-antikink pairs nucleate at the "V"-shaped points. Note that Fig. 5(b)
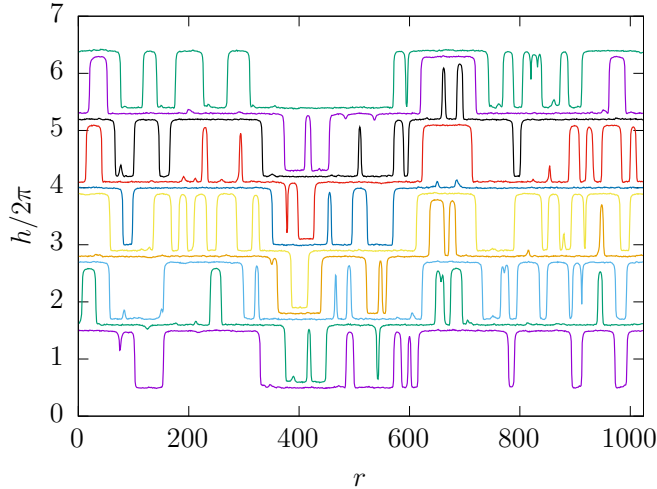
FIG. 4. A sequence of numerically generated configurations $h(r, t)$ for an elastic string of size $L = 1024$, $T = 5 \times 10^{-5}$, exactly at the critical force $f_c = 1$. Consecutive configurations at increasing times (from bottom to top) have been differently colored and slightly shifted vertically by ~ 0.1 for clarity.

can be described as a "contour plot" of the funcion $h(x, t)$, each contour (characterized by an increasing integer number ν) indicating the time at which the interface first reached the height $h = 2\pi\nu$. The space-time plot of Fig. 5(b) is a full picture of the dynamics of the string in spatial scales larger than the typical size of the kinks. Figure 5(b) hence reveals the sparse and localized activity of the interface.

In Fig. 6 we can qualitatively appreciate the kink dynamics at $f = f_c$ for different temperatures in the steady state. The four panels correspond to four different increasing temperatures. The space and time extent of the four panels is the same. We observe in particular that the slope of the straight segments (corresponding to kink propagation) has the same value c^{-1} for all temperatures. As described above the space-time segments describing kink trajectories form a
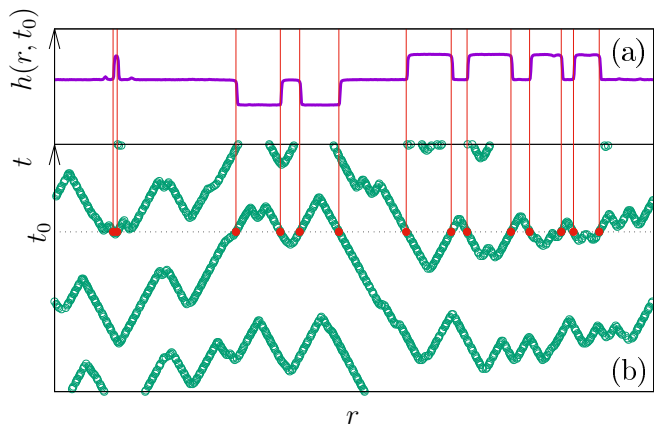

FIG. 5. (a) Snapshot of a configuration $h(r, t_0)$ of the interface at $t = t_0$, exactly at the critical force $f_c = 1$ and $T = 10^{-5}$, generated from Eq. (33) for $L = 1024$. (b) Kink trajectories in space time. Red dots correspond to kink positions at $t = t_0$. Dashed vertical lines show their correspondence with $h(r, t_0)$ kinks.
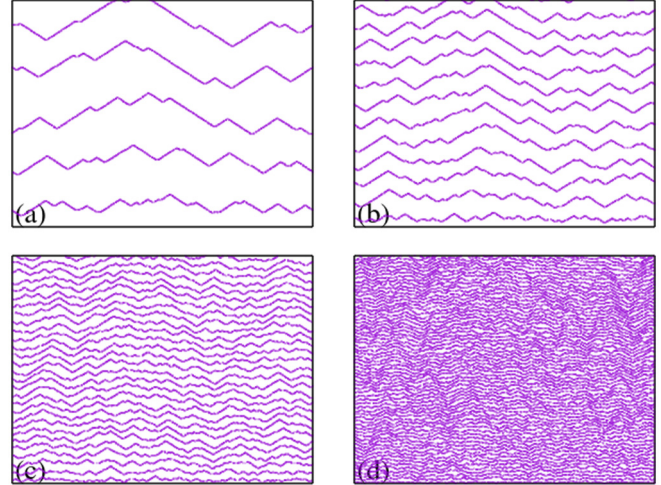

FIG. 6. Numerically generated kink trajectories exactly at the critical force for different temperatures, $T = 10^{-6}$ (a), $T = 10^{-5}$ (b), $T = 10^{-4}$ (c), and $T = 10^{-3}$ (d), for a string of size $L = 1024$. The vertical and horizontal directions are time and position, respectively, and have the same extent in the four panels. The time gaps between the zig-zagging contours formed by many kink and antikink trajectories arise naturally from the dynamics.

well-defined sequence of activity contours that percolate in space but are separated by distinguishable time gaps (i.e., different lines do not get close vertically in practice). It is worth stressing, however, that, in spite of these time gaps, the one-dimensional interface at the steady state is actually *never* completely trapped in a metastable state: For given time t a large-enough interface always has pairs of kinks evolving quasideterministically. In other words, a line with $t = $ const in space time always cuts the trajectory of some kinks in a thermodynamic system at any finite temperature. Another interesting property that can be appreciated in Fig. 6 is that increasing temperature increases both the space-time density of annihilation and creation events and decreases the time gaps, strongly suggesting a space-time-temperature scaling relation, which we will discuss now in detail.

In Sec. III, and working below the critical force, we considered the nucleation of kink-antikink pairs to occur at a rate R that was simply a function of temperature. This led to the estimation that the velocity interface is $v \sim R^{1/2}$ [Eq. (27)]. This analysis was appropriate because in that case there was a finite energy barrier to be surmounted, and the dynamics of this activation is statistically a Poisson process: If an attempt to climb the barrier has failed, then the next one has to start over, independently of how many previous attempts have been made. But right at f_c, the transition between successive bottleneck positions does not require the climbing of any energy barrier. The bottlenecks are characterized by a flat potential in which the deterministic force vanishes, and the transition time displays the typical time gap already seen in the single-particle case (Fig. 3). Therefore in this case the nucleation rate R previously used is not a useful concept. Instead, it will be useful to consider (as in the 0-dimensional case) the function F, which measures the time in which a kink-antikink pair is first observed starting with an originally flat interface at f_c.
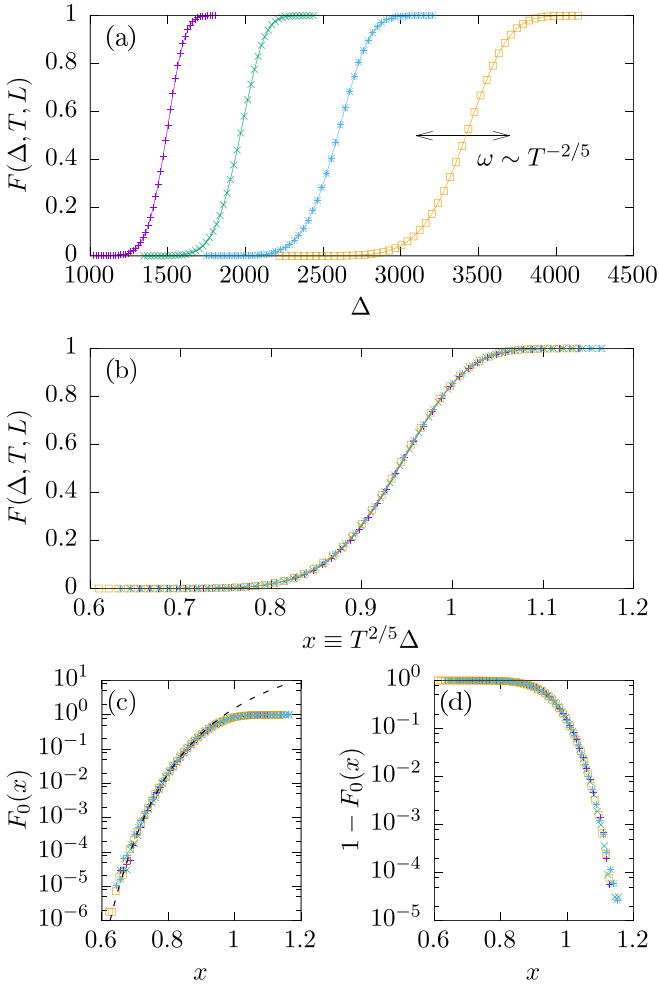
FIG. 7. Waiting-time cumulative distributions for the activation of the first pair of kinks in a flat ($d = 1$) elastic string exactly at $f = f_c$, for different temperatures T and string sizes L, such that $TL^{1/5} = $ const. (a) The rightmost curve corresponds to $L = 2^{16}$, $T = 1.25 \times 10^{-9}$, each following curve to the left doubles the temperature. (b) Master curve using the time-temperature-length scaling, $F(\Delta, T, L) \sim \tilde{F}(T^{2/(6-d)}\Delta, T^{1/(6-d)}L) \equiv F_0(T^{2/(6-d)}\Delta)$ in the case $d = 1$. (c) The dashed line $\sim \exp[-4.58/x^3]$ is an empiric fit of the left part of $F_0(x)$. (d) Detail of the right tail of $F_0(x)$, to be compared with the single-particle case in Fig. 3.

We consider a system of size L (with periodic boundary conditions) and start at $t = 0$ with a flat configuration at $h = h_0 < 0$. This configuration moves deterministically toward the saddle located at $h = 0$ and would remain there if $T = 0$. However, thermal fluctuations produce the surpassing of the saddle, and we determine the time Δ at which the first point of the interface is detected at some positive h_1, indicating a kink-antikink pair has been created. The value of Δ becomes large as $T \to 0$, and therefore the precise values of h_0 and h_1 are not important. We choose $h_0 = -1$, $h_1 = 1$. The numerical procedure is repeated many times to collect statistics of Δ values. Figure 7(a) shows the cumulative distribution function F of the first nucleation time Δ, for different temperatures T and system sizes L. The form of $F(\Delta, T, L)$ can be simplified using the general scaling theory of Sec. III, which can be applied to the present calculation without change, simply con-

sidering $\varepsilon \equiv 0$. Since F is a dimensionless function, it must remain the same when its arguments are changed according to the scaling in Sec. III. Therefore, we obtain:

$$F(\Delta, T, L) = \tilde{F}(T^{2/(6-d)}\Delta, T^{1/(6-d)}L). \quad (36)$$

Since $d = 1$, and we are fixing $LT^{1/5}$ in the simulations; for simplicity we will omit the L dependence everywhere and simply write $F(\Delta, T, L) = F_0(x)$ with $x \equiv T^{2/5}\Delta$ and $F_0(x)$ the master curve. In Fig. 7(b) we show the excellent collapse obtained for the different curves in Fig. 7(a) obtained using this scaling.

It is interesting to compare the tails of $F_0(x)$ for the string and the particle. In the single-particle case $F_0(x)$ is exponential for large x, while the elastic string displays a clear faster-than-exponential decay at large x. On the other hand, for small x, both cumulative distributions display a slower than exponential growth.

The results in Fig. 7 clearly display the "gap" effect in the nucleation time (also observed for the single-particle case in Fig. 3), pointing also to the fact that this nucleation cannot be considered anymore (as it was in the activated regime) a Poisson process. Thus the probability to nucleate a kink-antikink pair in a piece of interface at height $h = 2\pi\nu$ depends on how much time the surface has stayed at $2\pi\nu$ already. To get an idea of this phenomenon and its importance, it is worth looking again in Fig. 6 to the ubiquitous time gaps appearing in sequences of many contours for different temperatures. The rather well-defined values of the vertical gaps between different contours in the plot in Fig. 6 is a consequence of the fact that nucleation time cannot be arbitrarily small, as seen also in Fig. 7. The numerical results for the function F just presented will be useful in the next section to calculate the interface velocity at $f = f_c$.

2. $v(T)$ curve at $f = f_c$

Armed with the qualitative understanding of the dynamics we gained in the previous section (Sec. IV B 1), we can address quantitatively the expected form of the temperature dependence of the velocity v right ar f_c, namely the thermal rounding law. Referring to the plots in Fig. 6, the value of v is nothing more than 2π divided by the average temporal separation between successive contours, that we call Δ_0. We must estimate Δ_0 in order to calculate v as $v = 2\pi/\Delta_0$.

One may naively expect that Δ_0 is simply given by the average value of the nucleation time $\overline{\Delta}$ that can be extracted from the data in Fig. 7. However, this is not quite so. Kink-antikink pairs nucleated with particularly small values of Δ (at the left of the distribution in Fig. 7) will have a stronger influence and produce that $\Delta_0 < \overline{\Delta}$. In order to understand correctly this fact and its importance, let us consider the sketch in Fig. 8. In Fig. 8(a) we depict with the thick black line one of the contours (with label ν) already shown in Fig. 6. This contour represents, for all spatial positions, the time at which the interface reaches the height $2\pi\nu$. Suppose that each horizontal position in Fig. 8 represents a portion of the interface to which the analysis in Fig. 7 can be applied. This means that for each horizontal position we can draw a point from Fig. 7 and plot a *nominal time* at which a kink-antikink pair would be nucleated at that position. This is represented
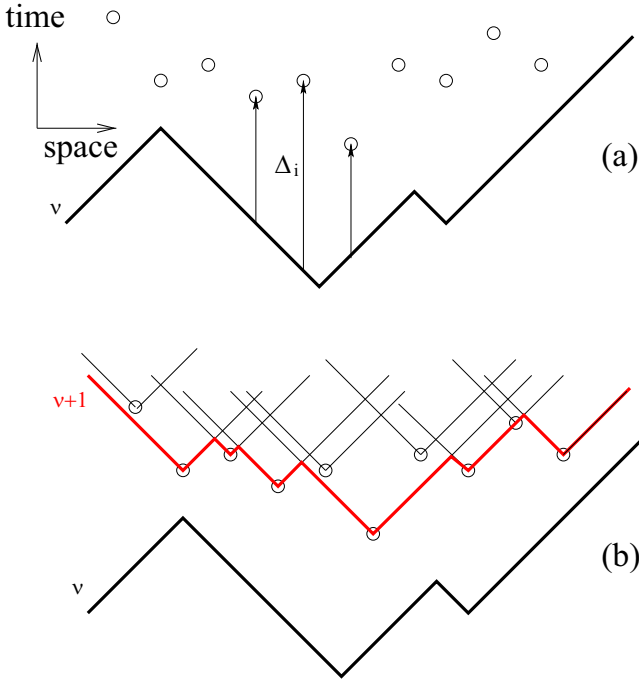
FIG. 8. (a) Thick line: Sketch of contour ν of the space-time configuration of an interface (see Fig. 6). In principle, at each spatial position, the next kink-antikink is nucleated at the time indicated by the small circles. (b) The actual $\nu + 1$ contour is constructed by kinks and antikinks emanating from the nucleation points. Only the earliest kink-antikink actually contribute to the contour $\nu + 1$ (shown in red). Notice that the average time position of contour $\nu + 1$ is smaller than the average time position of all circles.

in Fig. 8(a) as the open circles. The average temporal distance between contour ν and all open circles is simply the value $\overline{\Delta}$ extracted from the Fig. 7. However, each nucleation point generates a kink-antikink pair that propagates in the system as indicated in Fig. 8(b). The actual $\nu + 1$ contour is the lower envelope of all these kink-antikink pairs. It is apparent from Fig. 8 that the average time separation Δ_0 between contours ν and $\nu + 1$ is smaller than $\overline{\Delta}$.

In order to calculate Δ_0 explicitly we notice that the contour $\nu + 1$ is composed of kinks and antikinks originated in the lowest values of the nucleation times at all sites or, in other words, the lowest circles in Fig. 8. If M is the average number of sites affected by a single kink-antikink pair, then the typical value of Δ_0 corresponds to the typical value of the minimum of M variables Δ_i with cumulative distribution $F(\Delta, T)$ (the function plotted in Fig. 7). This minimum is roughly given by the condition

$$MF(\Delta_0, T) = 1, \tag{37}$$

and the velocity of the interface will be given by $v = 2\pi/\Delta_0$. The main temperature dependence of v comes from the temperature dependence of $F(\Delta_0, T)$. The temperature dependence of M will account for a logarithmic correction, as we will now see. From the numerical results in Fig. 7(c), $F(\Delta_0, T)$ can be very well approximated (particularly when $F \ll 1$) as

$$F(\Delta_0, T) \simeq \exp[-C/(T^{2/5}\Delta_0)^3] \tag{38}$$

with $C \simeq 4.58$ a numerical constant. Note that the form of the combination $T^{2/5}\Delta$ comes already from the scaling of time and temperature, in the analysis of Sec. III applied to the $d = 1$ case. The third power instead, is just a rough numerical fitting [see the dashed line in Fig. 7(c)]. The dependence of M on temperature is roughly given by the following argument: A kink-antikink starting at one of the lowest circles in Fig. 8 will be part of the $\nu + 1$ contour for a number of sites M, such that $M/c \sim \omega$, where ω is the width of the $F(\Delta, T)$ function. According to Eq. (38) ω scales with temperature as $\omega \sim T^{-2/5}$. Putting the pieces together, and since c is just a constant, this gives simply

$$M \sim T^{-2/5}. \tag{39}$$

Using now Eqs. (38) and (39) in Eq. (37) we finally obtain

$$v = c_1 T^{\frac{2}{5}}[-\ln(c_2 T)]^{\frac{1}{3}}, \tag{40}$$

where we have dig into c_1 and c_2 all unknown constants of the analysis. In general dimension d, the kink-antikink pair of the $d = 1$ case is replaced by a $(d - 1)$-dimensional domain wall describing a droplet boundary, allowing d-dimensional patches to advance from one position to the following in an isotropic way. The mechanism just described of nucleation, expansion and coalescence of defects qualitatively applies in general dimension and the expected form of v at f_c is

$$v = c_1 T^{\frac{2}{(6-d)}}[-\ln(c_2 T)]^{\delta}, \tag{41}$$

where the exponent δ of the logarithmic correction is 0 in $d = 0$ and $1/3$ in $d = 1$. For $d > 1$ we expect it to be different from zero, but we have not attempted a precise determination.

The result we have obtained for the dependence of $v(T)$ shows a main power-law dependence but also an important logarithmic correction that can have an important effect on experimentally observed values. Qualitatively, the origin of the two parts can be traced back to the particular dynamics of the problem. The $T^{2/(6-d)}$ factor in the velocity comes from the average transition time between bottleneck configurations at which the interface spends most of the time. The logarithmic factor is a consequence of the linear-in-time increase of the extent of the interface at position $2\pi\nu$ before nucleating the defect that will allow the transition to the $2\pi(\nu + 1)$ position (see Appendix B for a more formal derivation of the necessity of such a logarithmic correction, independently of the details of the dynamics).

We now check the form of $v(T)$ from Eq. (40) against numerical simulations. The results span seven orders of magnitude in temperature ($10^{-7} \leqslant T \leqslant 1$) in a large-enough system ($L = 2^{23}$) such that $T^{1/5}L \gg 1$ so to avoid finite-size effects (also implying a large number of evolving kinks at any instant). Figure 9(a) shows the results of a simulation in the full model at $f = f_c$. If we were trying to fit a power law, we would probably fit an exponent $\simeq 0.38$ (yellow line) at least in the left part of the figure. Yet our proposed behavior [Eq. (40)] produces a more satisfactory and consistent result. By fitting appropriately c_1 and c_2 we find the green curve, which fits the data in a much broader range of temperatures. This is even clearer in Fig. 9(b), where an effective power-law exponent as a function of temperature is obtained $\psi_{\text{eff}} \approx d \ln v/d \ln T$, using the method of consecutive slopes, and
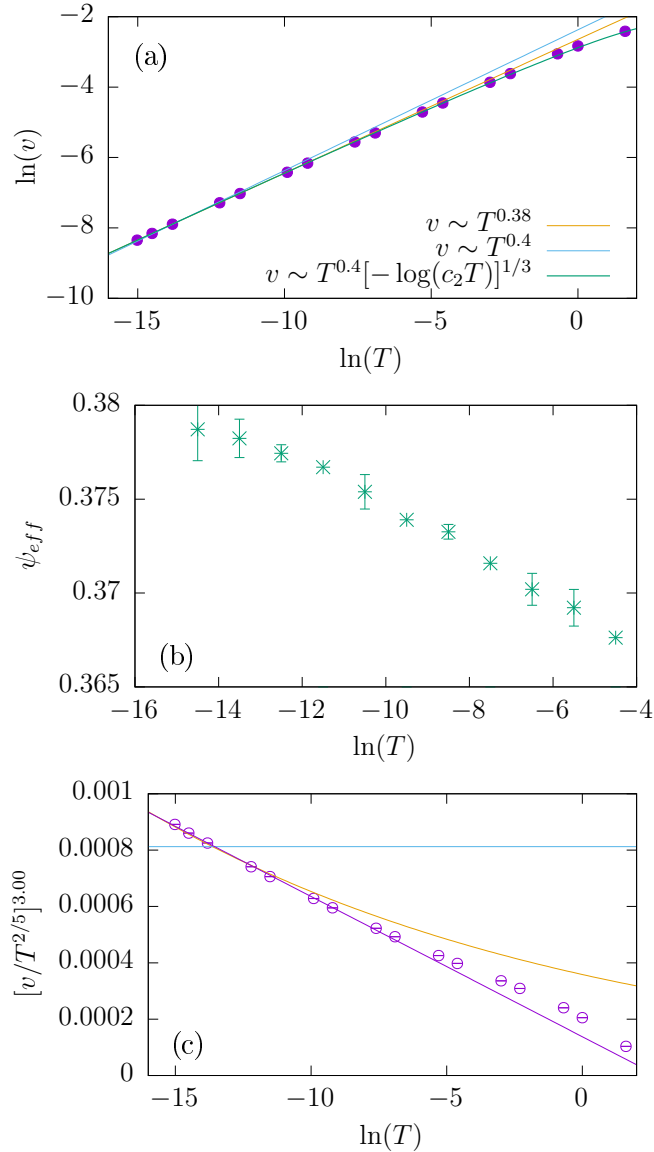
FIG. 9. (a) Velocity as a function of temperature ($T \in [10^{-7}, 10]$) at $f = f_c$, for an elastic string of size $L = 8\,388\,608$. The yellow line is a naive pure power-law fitting of the form $v \simeq T^{\psi_0}$, $\psi_0 \simeq 0.38$. The green line is a fit from our Eq. (40), consisting in a power law $T^{2/(6-d)} = T^{0.4}$ multiplied by a logarithmic correction. The blue line, with slope $2/(6-d) = 0.4$, is used only for reference. (b) Effective power-law exponent $\psi_{\text{eff}} \approx d \ln v / d \ln T$, using the method of consecutive slopes (see text). (c) The same results as in (a) but plotted as $[v/T^{0.4}]^3$ vs $\ln T$, highlighting the logarithmic corrections. The accuracy of Eq. (40) is very good, except for large temperatures where some nonconsidered effects enter into play.

fitting pure power law in windows of size $[T - \Delta T, T + \Delta T]$ with $\ln[(T + \Delta T)/(T - \Delta T)] = 3$. This effective exponent shows a dependence compatible with very slow convergence to 0.4 when $T \to 0$, as Eq. (40) implies. Also, in Fig. 9(c) the data are plotted in such a way that they must follow a straight line if Eq. (40) is followed. We see in fact that they follow very well this behavior, except for large temperatures in which some effects not considered in our analysis enter into play

(particularly when temperature becomes a sizable fraction of the total amplitude of the corrugation potential and the system crossovers to the fast-flow regime where $v \sim f_c$).

V. CONCLUSIONS

The naive analogy of the depinning transition with standard phase transitions suggests that the average velocity of an extended elastic manifold exactly at the threshold should scale as $v \sim T^{\psi}$ for small temperatures T, with ψ the thermal rounding exponent. Pioneer arguments testing this idea, and yielding the first nontrivial predictions for ψ, were first given in the context of charge density wave models with quenched disorder [19,22,56] and later proposed for models of disordered elastic interfaces. In particular, they led to the relation $\psi = \beta/\alpha$, with β the zero temperature velocity exponent [$v(f, T = 0) \sim (f - f_c)^{\beta}$] and α the barrier exponent describing how barriers U for nucleation of forward-moving modes vanish approaching the depinning threshold from below [$U(f) \sim (f_c - f)^{\alpha}$]. In spite of several subsequent analytical [26,57,58], numerical [20,21,29,59–62] (some of them with different predictions for ψ), and experimental [20,63,64] studies, a proper understanding of the thermal rounding of the depinning transition remains elusive.

We have analyzed a simple version model of the depinning transition, namely the interface in a washboard potential, and found that right at the threshold the velocity follows by Eq. (41), which contains an important logarithmic correction (when $d \neq 0$) compared with the pure power-law behavior. We have shown that the logarithmic correction in this model can be physically explained in terms of a competition between the droplet nucleations (bounded by a kink-antikink pair in $d = 1$ or a $d - 1$-dimensional domain wall for $d > 1$) and the expanding deterministic motion they immediately trigger. In either case the later deterministic motion is hence not only responsible for displacing pieces of the interface one period further but also responsible for the deactivation of the nucleation in nearby sites (see Fig. 8). It is worth stressing that the left tail of the waiting time distribution for nucleation plays a fundamental role in producing logarithmic corrections. At this respect we note that the characteristic space-time structure we observe at the depinning transition (see Fig. 6) is clearly different from the one observed in the polynuclear growth model [65] (and other similar solid-on-solid growth models) where droplet nucleations are randomly sampled from a Poisson distribution before expanding them. As shown in Fig. 7, a Poisson distribution does not apply at all to the thermally assisted dynamics at the critical force. Interestingly, the exponent $2/(6 - d)$ in Eq. (41) still agrees exactly with the relation $\psi = \beta/\alpha$ (with $\beta = 1/2$ and $\alpha = (6 - d)/4$) proposed in Ref. [22]. Furthermore, we have shown that the same prefactor exponent β/α actually holds for an infinite family of periodic potentials with different values of α and β (Appendix A). Our results hence predict that, in practice, the effective thermal rounding exponent will approach β/α slowly and from below in the limit of small temperatures.

Based on the above findings, we conjecture that the thermal rounding of the depinning transition in the more generic case of interfaces in disordered pinning landscapes for $d > 0$ also

displays logarithmic corrections, which may be written as

$$v = c_1 T^{\beta/\alpha}[-\ln(c_2 T)]^{\delta}, \tag{42}$$

where $\delta \geqslant 0$ is a new exponent describing the left tail (or "pseudogap") of the waiting time distribution for nucleation of localized modes exactly at the critical force. Such modes may be related to the marginally stable localized (at the Larkin length scale) soft modes found at the critical depinning configuration [66]. In this scenario, the deterministic expansion of thermally nucleated droplets would be replaced by the analogous avalanche motion observed near the depinning threshold. Noteworthy, some interface models with disorder gave already evidence of logarithmic corrections [21]. Testing this conjecture more broadly may help to advance our understanding of the thermal rounding of the depinning transition of elastic manifolds.

ACKNOWLEDGMENTS

APPENDIX A: GENERALIZATION OF THE NUCLEATION RATE SCALING AND THERMAL ROUNDING

Here we consider the motion of a flat interface segment near the depinning transition ($f = f_c - \varepsilon$) using a more general form for the bottleneck at $h = 0$,

$$\frac{\partial h(r)}{\partial t} = h^{\gamma} - \varepsilon + \nabla^2 h + \sqrt{T}\eta(t, r) \tag{A1}$$

with γ characterizing the normal form of the periodic force $-V'(h) \approx -h^{\gamma}$ around $h = 0$ and all its periodic images. Using the same arguments leading to 11 we now arrive at its generalization,

$$\varepsilon \to \tilde{\varepsilon} \equiv k\varepsilon, \tag{A2}$$

$$h \to \tilde{h} \equiv k^{\frac{1}{\gamma}}h, \tag{A3}$$

$$t \to \tilde{t} \equiv k^{\frac{1}{\gamma}-1}t, \tag{A4}$$

$$z \to \tilde{z} \equiv k^{\frac{1-\gamma}{2\gamma}}z, \tag{A5}$$

$$T \to \tilde{T} \equiv k^{2-\frac{(2+d)(\gamma-1)}{2\gamma}}T, \tag{A6}$$

which reduces for $\gamma = 2$ to Eq. (11). Repeating the same steps than for $\gamma = 2$ we obtain the generalized γ-dependent nucleation rate per unit volume,

$$R(T, \varepsilon, L) = \varepsilon^{\frac{(2+d)(\gamma-1)}{2\gamma}} R\left(T/\varepsilon^{2-\frac{(2+d)(\gamma-1)}{2\gamma}}, 1, LT^{\frac{\gamma-1}{2\gamma-\gamma d+d+2}}\right). \tag{A7}$$

Alternatively, for large sizes $LT^{\frac{\gamma-1}{2\gamma-\gamma d+d+2}} \gg 1$, we can write

$$R(T, \varepsilon) = T^{\frac{(\gamma-1)(d+2)}{2(\gamma+1)-(\gamma-1)d}} \mathcal{F}\left(\varepsilon^{2-\frac{(2+d)(\gamma-1)}{2\gamma}}/T\right) \tag{A8}$$

with $\mathcal{F}(x)$ a master function,

$$\mathcal{F}(x) \equiv x^{\frac{(\gamma-1)(d+2)}{2(\gamma+1)-(\gamma-1)d}} R(1/x, 1, \infty). \tag{A9}$$
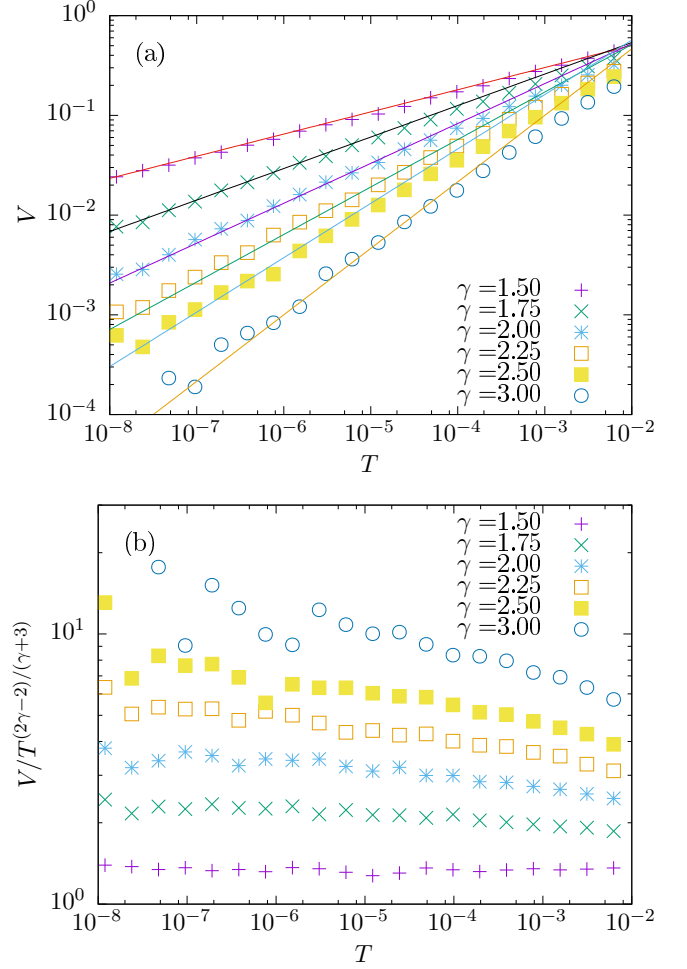

FIG. 10. (a) Velocity vs temperature at the depinning transition for an elastic string ($d = 1$) of size $L = 132\,768$ in a periodic potential characterized by the normal form exponent γ. Larger γ imply shallower force minima (see text). Lines display the power-law behavior $v \sim T^{\psi(\gamma,d)}$, where $\psi = \frac{2\gamma-2}{2\gamma-\gamma d+d+2}$. (b) Same data but highlighting the corrections to the power law by plotting $v/T^{\psi(\gamma,d=1)}$ vs T.

At $T = 0$ is easy to see that the velocity at the depinning transition in this family of periodic potentials is $v \sim (f - f_c)^{\beta}$ with $\beta = 1 - 1/\gamma$, since the problem reduces to the particle case [21]. If we use that $\psi \approx \beta/\alpha$, then we find the thermal rounding exponent $\psi = \frac{2\gamma-2}{2\gamma-\gamma d+d+2}$. In $d = 1$ we get in particular $\psi = \frac{2\gamma-2}{\gamma+3}$, so for $\gamma = 2$ we have $\psi = \frac{2}{5}$.

In Fig. 10 we compare with v data at $f_c = 1$, vs temperature T. As can be appreciated in Fig. 10(a) the ansatz $\psi = \frac{2\gamma-2}{2\gamma-\gamma d+d+2}$ works reasonably, but corrections to the pure law scaling manifest already for temperatures $T > 10^{-4}$ (in units of the microscopic energy scale which we have set to unity). Interestingly, as shown in Fig. 10(b), these corrections are accentuated for larger γ, corresponding to shallower bottlenecks $h^{\gamma} - \epsilon$ around $h = 0$. As we have discussed for $\gamma = 2$ case, logarithmic corrections are originated in the wide distribution of the nucleation times. The enhancement of corrections for increasing values of γ indicates that this distribution becomes wider as γ increases.
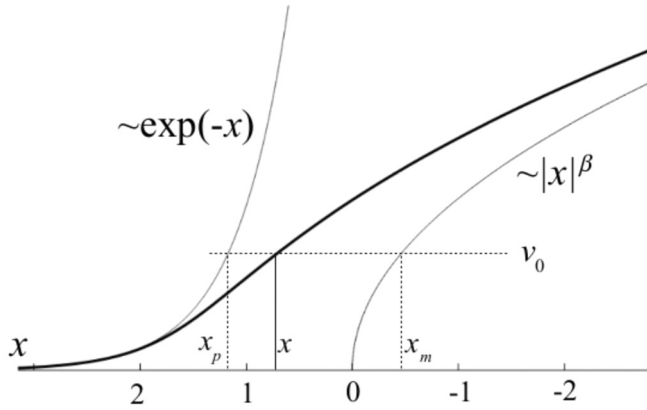
FIG. 11. Sketch of a function of which we know its limiting forms v_p and v_m as $x \to \pm\infty$. A possible interpolating function $v(x)$ for all x consists in fixing some value v_0, and choosing x such that $x \equiv v_p^{-1}(v_0) + v_m^{-1}(v_0)$.

APPENDIX B: AN INDEPENDENT JUSTIFICATION FOR THE EXISTENCE OF LOGARITHMIC CORRECTIONS AT $f = f_c$

In the main part of this work, we have analyzed the velocity of an interface in a washboard potential at finite temperatures. When the driving force f is larger than the critical force f_c, the limiting velocity as $T \to 0$ corresponds to the athermal limit $v \sim (f - f_c)^\beta$, with $\beta = 1/2$. In the case in which $f < f_c$, and for $d = 1$ the velocity vanishes in the limit $T \to 0$ following an activation scaling that includes an Arrhenius factor of the form $\sim \exp(-C|f - f_c|^{5/4}/T)$. We then analyzed the behavior of the velocity right at the critical point, namely $f = f_c$, showing that this velocity has a dominant power-law term in T, plus some logarithmic correction.

In the present Appendix, we want to show formally why this kind of logarithmic correction appears naturally in this problem. To this end, we pose the following mathematical problem which, however, is clearly related to the physical problem we have studied. Suppose we consider a function v (to be associated to the velocity of the interface) as a function of $x \equiv f_c - f$, and temperature T. Suppose we know that $v(x, T) \to |x|^\beta$ as $x \to -\infty$ [67] for any T. Also, suppose that as $x \to +\infty$ we know $v(x, T) \simeq T^A \exp(-x^\alpha/T)$ (compare with Eq. (30); for simplicity we do not consider here the possibility of a preexponential power of x). The problem we pose is to find a consistent family of functions $v(x, T)$ for all x, satisfying the previous limiting forms. Once the family of functions has been found, we are mainly interested in the thermal rounding function $v(x = 0, T)$.

In this very general form there will be of course many different solutions to the problem. Our goal here is to show how in one possibly (arguable one of the simplest) solutions that can be obtained, a logarithmic correction in the thermal rounding function appears, which is originated in the expo-

nential form of the limiting function for $x \to +\infty$. In fact, in Fig. 11 we can see the formal problem we are posing. There we see plotted with thin lines the two limiting functions for $x \to \pm\infty$. We call them v_p and v_m for concreteness. The thick line is an example of a possible function interpolating between these two limits. One simple form of analytically obtaining one such interpolation function consists in the following: Fixing a generic value v_0 of v ($v_0 > 0$) we obtain the two points x_p and x_m such that $x_p = v_p^{-1}(v_0)$, $x_m = v_m^{-1}(v_0)$. Then we define the interpolating function $v(x)$, choosing $x = x_p + x_m$. Being more explicit, we define the inverse function v^{-1} as

$$v^{-1}(v_0) = v_p^{-1}(v_0) + v_m^{-1}(v_0). \tag{B1}$$

Using the explicit forms $v_p(x) \equiv T^A \exp(-x^\alpha/T)$, $v_m(x) \equiv |x|^\beta$ we obtain

$$x \equiv v^{-1}(v_0) = v_0^{1/\beta} + [-T \ln(v_0 T^{-A})]^{1/\alpha}. \tag{B2}$$

Let us note the following. As the two terms of this definition have positive derivatives, the function v^{-1} can be reinverted to obtain a single valued $v_0(x) \equiv v(x)$ function. In addition, when $v_0 \to \infty$, the first term in (B2) dominates, whereas when $v_0 \to 0$ is the second term that dominates. Then the two limits of the function $v(x)$ are satisfied.

Expression (B2) cannot be inverted analytically in general, but we can advance further considering the thermal rounding function, namely the case $x = v^{-1}(v_0) = 0$. We obtain

$$0 = v^{1/\beta} + [-T \ln(v T^{-A})]^{1/\alpha} \tag{B3}$$

or

$$v^{\alpha/\beta} = -T \ln(v T^{-A}). \tag{B4}$$

This expression can be considered as it stands, as an implicit form of the thermal rounding curve. Alternatively we can get an explicit form by working iteratively: Taking into account the slow variation of the logarithmic factor, we can solve it first by considering the log term is a constant, to obtain $v \simeq (CT)^{\beta/\alpha}$, and then using this zero-order approximation inside the log in Eq. (B4), to obtain:

$$v \simeq T^{\beta/\alpha}\{-\ln[(CT)^{\beta/\alpha} T^{-A}]\}^{\beta/\alpha}. \tag{B5}$$

Either from this approximate expression, or from the general solution [Eq. (B4)], we can see that in the particular case in which $A = \beta/\alpha$, the logarithmic correction vanishes and the solution is $v \sim T^{\beta/\alpha}$. This is just the case in which the activation form of the function we are looking for in the limit $x \to -\infty$ is compatible (in the sense discussed at the end of Sec. III B) with the form $|x|^\beta$ in the limit $x \to \infty$. Except in this particular case, logarithmic effects are expected.

We see that the appearance of a logarithmic correction seems to be a very general result associated to (i) the impossibility of fitting the two limiting expressions for $x \to \pm\infty$ with a single scaling relation [as the one in Eq. (31)] and (ii) the exponential activation form for $x \to \infty$, whose inversion is responsible for the logarithmic factor in the thermal rounding law.

[1] J. Ferré, P. J. Metaxas, A. Mougin, J.-P. Jamet, J. Gorchon, and V. Jeudy, C. R. Phys. **14**, 651 (2013).

[2] W. Kleemann, Annu. Rev. Mater. Res. **37**, 415 (2007).

[3] P. Paruch and J. Guyonnet, C. R. Phys. **14**, 667 (2013).

[4] D. Bonamy, S. Santucci, and L. Ponson, Phys. Rev. Lett. **101**, 045501 (2008).

[5] L. Ponson, Phys. Rev. Lett. **103**, 055501 (2009).

[6] C. Le Priol, J. Chopin, P. Le Doussal, L. Ponson, and A. Rosso, Phys. Rev. Lett. **124**, 065501 (2020).

[7] J. F. Joanny and P. G. de Gennes, J. Chem. Phys. **81**, 552 (1984).

[8] S. Moulinet, A. Rosso, W. Krauth, and E. Rolley, Phys. Rev. E **69**, 035103(R) (2004).

[9] P. L. Doussal, K. J. Wiese, S. Moulinet, and E. Rolley, Europhys. Lett. **87**, 56001.

[10] E. A. Jagla and A. B. Kolton, J. Geophys. Res.: Solid Earth **115** (2010).

[11] E. A. Jagla, F. P. Landes, and A. Rosso, Phys. Rev. Lett. **112**, 174301 (2014).

[12] M. Tinkham, *Introduction to Superconductivity*, 2nd ed. (Dover, London, 2004).

[13] A. Pérez-Junquera, V. I. Marconi, A. B. Kolton, L. M. Álvarez-Prado, Y. Souche, A. Alija, M. Vélez, J. V. Anguita, J. M. Alameda, J. I. Martín, and J. M. R. Parrondo, Phys. Rev. Lett. **100**, 037203 (2008).

[14] V. I. Marconi, A. B. Kolton, J. A. Capitán, J. A. Cuesta, A. Pérez-Junquera, M. Vélez, J. I. Martín, and J. M. R. Parrondo, Phys. Rev. B **83**, 214403 (2011).

[15] P. J. Metaxas, P.-J. Zermatten, R. L. Novak, S. Rohart, J.-P. Jamet, R. Weil, J. Ferré, A. Mougin, R. L. Stamps, G. Gaudin, V. Baltz, and B. Rodmacq, J. Appl. Phys. **113**, 073906 (2013).

[16] D. S. Fisher, Phys. Rep. **301**, 113 (1998).

[17] M. Kardar, Phys. Rep. **301**, 85 (1998).

[18] S. Brazovskii and T. Nattermann, Adv. Phys. **53**, 177 (2004).

[19] D. S. Fisher, Phys. Rev. B **31**, 1396 (1985).

[20] S. Bustingorry, A. B. Kolton, and T. Giamarchi, Phys. Rev. E **85**, 021144 (2012).

[21] V. H. Purrello, J. L. Iguain, A. B. Kolton, and E. A. Jagla, Phys. Rev. E **96**, 022112 (2017).

[22] A. A. Middleton, Phys. Rev. B **45**, 9465 (1992).

[23] P. Le Doussal, K. J. Wiese, and P. Chauve, Phys. Rev. B **66**, 174201 (2002).

[24] A. Rosso, P. Le Doussal, and K. J. Wiese, Phys. Rev. B **75**, 220201(R) (2007).

[25] P. Le Doussal and K. J. Wiese, Phys. Rev. E **79**, 051106 (2009).

[26] P. Chauve, T. Giamarchi, and P. Le Doussal, Phys. Rev. B **62**, 6241 (2000).

[27] A. B. Kolton, A. Rosso, T. Giamarchi, and W. Krauth, Phys. Rev. Lett. **97**, 057001 (2006).

[28] A. B. Kolton, A. Rosso, T. Giamarchi, and W. Krauth, Phys. Rev. B **79**, 184207 (2009).

[29] E. E. Ferrero, S. Bustingorry, A. B. Kolton, and A. Rosso, C. R. Phys. **14**, 641 (2013).

[30] D. Hull and D. J. Bacon, *Introduction to Dislocations*, Vol. 37 (Elsevier, Amsterdam, 2011).

[31] M. Büttiker and R. Landauer, Phys. Rev. A **23**, 1397 (1981).

[32] P. M. Chaikin and T. C. Lubensky, *Principles of Condensed Matter Physics* (Cambridge University Press, Cambridge, UK, 1995).

[33] T. Hwa, M. Kardar, and M. Paczuski, Phys. Rev. Lett. **66**, 441 (1991).

[34] A.-L. Barabási and H. E. Stanley, *Fractal Concepts in Surface Growth* (Cambridge University Press, Cambridge, UK, 1995).

[35] G. Blatter, M. V. Feigel'man, V. B. Geshkenbein, A. I. Larkin, and V. M. Vinokur, Rev. Mod. Phys. **66**, 1125 (1994).

[36] T. Nattermann and S. Scheidl, Adv. Phys. **49**, 607 (2000).

[37] T. Giamarchi and S. Bhattacharya, in *High Magnetic Fields*, edited by C. Berthier, L. P. Lévy, and G. Martinez, Lecture Notes in Physics, Vol. 595 (Springer-Verlag, Berlin, 2002), pp. 314–360.

[38] P. Le Doussal, Int. J. Mod. Phys. B **24**, 3855 (2010).

[39] C. H. Bennett, M. Büttiker, R. Landauer, and H. Thomas, J. Stat. Phys. **24**, 419 (1981).

[40] O. M. Braun and Y. S. Kivshar, *The Frenkel-Kontorova Model: Concepts, Methods, and Applications* (Springer Science & Business Media, New York, 2013).

[41] V. L. Popov and J. Gray, ZAMM-J. Appl. Math. Mech./Z. Angew. Math. Mech. **92**, 683 (2012).

[42] G. Tatara and H. Kohno, Phys. Rev. Lett. **92**, 086601 (2004).

[43] V. Lecomte, S. E. Barnes, J.-P. Eckmann, and T. Giamarchi, Phys. Rev. B **80**, 054413 (2009).

[44] S. E. Barnes, J.-P. Eckmann, T. Giamarchi, and V. Lecomte, Nonlinearity **25**, 1427 (2012).

[45] Even if the interface is started in an arbitrary $h(r)$ configuration, it gradually flattens, and for $t \to \infty$ the interface becomes flat if $T = 0$.

[46] A. M. Ettouhami and L. Radzihovsky, Phys. Rev. B **67**, 115412 (2003).

[47] We are implicitly assuming here that $V(h) - fh$ is quadratic around their minima. For a more general situation see Appendix A.

[48] J. S. Langer, Phys. Rev. Lett. **21**, 973 (1968).

[49] If the size of the optimal patch becomes of the order of the interface size a dimensional crossover is expected towards the zero dimensional or single particle result $E_{\max} \to \varepsilon^{3/2}$.

[50] V. Ambegaokar and B. I. Halperin, Phys. Rev. Lett. **22**, 1364 (1969).

[51] A. R. Bishop and S. E. Trullinger, Phys. Rev. B **17**, 2175 (1978).

[52] The elastic force at the center of the kink is approximately zero, so it is only acted by the driving force f_c. In a small time interval δt, the interface at the kink position advances $\delta h = f_c \delta t$ in the vertical direction and $\delta x \approx \delta h \xi / 2\pi$ in the horizontal direction. Therefore $c \approx f_c \xi / 2\pi$.

[53] S. Habib and G. Lythe, Phys. Rev. Lett. **84**, 1070 (2000).

[54] As a matter of definition, the values of Δ are calculated as the time interval between the time h crosses the value $2\pi(n - 1/2)$ and the time in which it crosses the value $2\pi(n + 1/2)$.

[55] The strong decay of $f(x)$ we observe by decreasing x and small temperatures makes it that in practice, it can be considered as a hard gap.

[56] A. A. Middleton, Phys. Rev. Lett. **68**, 670 (1992).

[57] T. Nattermann, V. Pokrovsky, and V. M. Vinokur, Phys. Rev. Lett. **87**, 197005 (2001).

[58] M. Müller, D. A. Gorokhov, and G. Blatter, Phys. Rev. B **63**, 184305 (2001).

[59] L.-W. Chen and M. C. Marchetti, Phys. Rev. B **51**, 6296 (1995).

[60] L. Roters, A. Hucht, S. Lübeck, U. Nowak, and K. D. Usadel, Phys. Rev. E **60**, 5202 (1999).

[61] S. Bustingorry, A. B. Kolton, and T. Giamarchi, Europhys. Lett. **81**, 26005 (2007).

[62] S. Bustingorry, A. Kolton, A. Rosso, W. Krauth, and T. Giamarchi, Phys. B: Condens. Matter **404**, 444 (2009).

[63] J. Gorchon, S. Bustingorry, J. Ferré, V. Jeudy, A. B. Kolton, and T. Giamarchi, Phys. Rev. Lett. **113**, 027205 (2014).

[64] R. Diaz Pardo, W. Savero Torres, A. B. Kolton, S. Bustingorry, and V. Jeudy, Phys. Rev. B **95**, 184434 (2017).

[65] N. Goldenfeld, J. Phys. A: Math. Gen. **17**, 2807 (1984).

[66] X. Cao, S. Bouzat, A. B. Kolton, and A. Rosso, Phys. Rev. E **97**, 022118 (2018).

[67] In the real problem of the interface, the form $v \sim |x|^\beta$ does not really hold in the $x \rightarrow -\infty$ limit. However, since we are interested in a small neighborhood of $T = 0$, there will always be a range for which $|x|$ is "sufficiently large," and $v \sim |x|^\beta$ holds.